Laboratory observations of enhanced entrainment in dense overflows in the presence of submarine canyons and ridges.

A. K. Wåhlin, E. Darelius, C. Cenedese & G. F. Lane-Serff

Abstract.

The continental slopes in the oceans are often covered by small-scale topographic features such as submarine canyons and ridges. When dense plumes, flowing geostrophically along the slope, encounter such features they may be steered downslope inside and alongside the topography. A set of laboratory experiments was conducted at the rotating Coriolis platform to investigate the effect of small-scale topography on plume mixing. A dense water source was placed on top of a slope, and experiments were repeated with three topographies: a smooth slope, a slope with a ridge, and a slope with a canyon. Three flow regimes were studied: laminar, waves, and eddies. When a ridge or a canyon were present on the slope, the dense plume was steered downslope and instabilities developed along the ridge and canyon wall. This happened regardless of the flow characteristics on the smooth slope. Froude and Reynolds numbers were estimated, and were found to be higher for the topographically steered flow than for flow on smooth topography. The stratification in the collecting basin was monitored and the mixing inferred. The total mixing and the entrainment rate increased when a ridge or a canyon were present. The difference in mixing levels between the regimes was smaller when topography was present, indicating that it was the small-scale topography and not the large-scale characteristics of the flow that determined the properties of the product water.

1. Introduction.

Density currents supply bottom water to the ocean basins of the world, and the processes by which these mix and become diluted with the ambient water influence the basin stratification. It has been shown in laboratory experiments (e.g. Baines and Turner, 1969; Baines 2001, 2005; Wells & Wettlaufer, 2005, 2007) that an entraining plume builds a stratification in the basin that it 'feeds', and that the mixing in the plume determines the characteristics of the stratification in the basin. The sensitivity of ocean stratification to plume entrainment and how this is parameterized, has also been studied in regional ocean models (e.g. Chang et al., 2005), and in more idealized basins and models (e.g. Wåhlin and Cenedese, 2006; Hughes and Griffiths, 2006).

Turbulent mixing in stratified shear flows increases with decreasing Richardson number *Ri*, i.e. the ratio of the buoyancy frequency and the velocity shear. When bulk properties of a dense overflow are considered, it is more convenient to consider a bulk Richardson number, or the Froude number *Fr* which is related to *Ri* by $Fr = \dfrac{1}{Ri^2} = \dfrac{u}{\sqrt{g'h}}$, where *u*,

g', and *h* are the characteristic overflow velocity, reduced gravitational acceleration, and height, respectively. Laboratory plume studies (e.g. Ellison and Turner, 1959; Davies et al., 2002, Cenedese et al., 2004; Cenedese and Adduce, 2008) show that the entrainment rate increases with *Fr*. The same dependency is found in the ocean (e.g. Girton and Sanford, 2003; Price and Baringer, 1994). In one-dimensional 'streamtube' descriptions of the plume (e.g. Smith, 1975 and Price and Baringer, 1994) the entrainment rate depends strongly on the average slope of the bottom (Wåhlin and Cenedese, 2006).

Small-scale topographic features, such as submarine ridges and canyons, can steer dense water downslope alongside them. This has been observed in the Wyville Thompson

Ridge overflow (Sherwin and Turrell 2005; Sherwin et al., 2008), in the Adriatic Sea (Vilibic et al. 2004), in the Filchner overflow (Foldvik et al., 2004; Darelius et al., 2008), in laboratory experiments (Baines and Condie, 1998; Kämpf, 2005; Davies et al., 2006; Darelius, 2008) and in numerical models of dense outflows (Jiang and Garwood 1998; Kämpf and Fohrmann, 2000). As the water is steered downslope by the topography, the plume thickness and downslope velocity, and thereby the Froude number, change. Furthermore, the plume path and the distance over which entrainment occurs decreases for a topographically steered plume. The aim of the present study is to investigate to what extent small-scale topography affects the mixing in a dense overflow.

A set of laboratory experiment was conducted at the rotating Coriolis platform in Grenoble. Three parameter regimes, producing a laminar flow, a flow with roll waves, and a flow with eddies, were investigated for three different topographies. Cenedese at al. (2004) identified boundaries for these three regimes using the Froude number and the Ekman number, Ek, which is the ratio between the Ekman layer thickness and the plume thickness. A laminar flow was observed for $Fr < 1$. Under supercritical conditions with $Fr \geq 1$ and $0.05 < Ek < 5$, quasi-two dimensional billow structures, so called roll waves, were observed to form and propagate at an almost constant speed in the same direction as the bottom plume. The eddy regime occurs for $Fr < 1$ and $0.01 < Ek < 0.1$.

The experiments in each regime were performed on the smooth slope first, and then repeated twice, first with a submarine ridge, and then with a canyon positioned on the slope. The total mixing in the dense current over the slope was measured by sampling the basin water with vertically traversing probes every 5 minutes. This method appears to give a reliable estimate of the mixing provided the length of the slope exceeds the

frictional drainage length described in Lane-Serff and Baines (1998). In all three regimes, the total mixing is larger when small-scale topography was present on the slope than when it was not. This indicates that the acceleration of the dense current due to the topography outweighs the effect of the shortened plume path.

2. Experimental set-up.

The experiments were conducted on the Coriolis rotating platform, in a 13 m diameter tank. Figure 1 shows a sketch of the experimental setup. A sloping bottom, making an angle $\alpha = 6°$ with the horizontal (i.e. $s = \tan \alpha = 0.1$) and measuring 8 x 2.5 m was placed in the tank. The slope was connected to a 25 cm high horizontal shelf on one side. On the other side, at the bottom of the slope, a semi-circular basin was delimited by two vertical false walls and the outer tank circular wall. The gray area in Fig. 1c indicates the position of a removable section, where the smooth slope could be replaced by a canyon or a ridge. The ridge/canyon was 16 cm wide and 10 cm high/deep, and oriented perpendicular to the along-slope direction. A dense water source was placed on the top right side of the slope (looking upslope), 25 cm downslope from the shelf break. The source consisted of a 2.5 cm high and 20 cm wide rectangular plastic box filled with horsehair and an assemblage of thin (0.5 cm in diameter) plastic tubes through which the dense water flowed (Fig. 1b). The source width is not thought to have any dynamical effect, as suggested by experiments on a cone with a circular source (Sutherland et al., 2004) or by experiments with varying source width (Lane-Serff and Baines, 1998). A localized

source, instead of a broad distributed source, was used since it better represent the localized sources of dense water (e.g. Denmark Strait) observed in the ocean.

The tank was initially filled with fresh water to a depth D and spun up to a rotation period $T = 60$ s, equivalent to a Coriolis parameter $f = 0.21$ s^{-1}. The density of the injected water, ρ_0, was either (approximately) 0.04% or 0.1% denser than the ambient fluid, which corresponds to a reduced gravitational acceleration, g', of 0.004 m/s^2 and 0.01 m/s^2, respectively. At the start of the experiment the source was opened, releasing saline water continuously with a flow rate $Q_0 \approx 10$ l/min. The ambient water depth was kept constant by an open surface drain, which could be adjusted vertically, on the opposite side of the tank. The flow was visualized by coloring the source water red and videotaping it from above. The dye was added to the dense water using a separate pump with a flow rate that could be adjusted manually, hence it was possible to switch the dye source on and off during an experiment. The salinity in the enclosed basin was monitored with two vertically traversing probes, see Figure 1c for position. The probes were lowered with a speed of 1cm/s making one profile every 5 minutes during the course of the experiments. Only data recorded during the downcasts are considered here.

The source flow rate, density, and ambient water depth were tuned in order to produce three different flow regimes characterized by laminar flow, roll waves, and eddies (Cenedese et al., 2004). In addition, two criteria had to be fulfilled: (1) The frictional drainage length L_D (Lane-Serff and Baines, 1998),

$$L_D = \frac{Q_0 f^{\frac{3}{2}}}{g' s \sqrt{2\nu}}, \tag{1}$$

where ν is the kinematic viscosity, had to be smaller than the length of the slope (8 m);

and (2) The source flow rate, Q_0, had to be smaller than the maximum transport that the canyon/ridge can channel downslope, i.e. the transport capacity Q_C (see Appendix). Table 1 shows the ambient water depth and the density difference used to obtain the three regimes, together with L_D, Q_C, and the Nof velocity

$$U_N = \frac{g's}{f} .$$ (2)

Estimates of the bulk plume velocity obtained from the videotapes show that the actual velocity was up to 30 % smaller than U_N, as also observed by Cenedese and Adduce (2008). Since no accurate velocity measurements were performed, the Nof velocity is taken as representative for the plume.

For each regime, three experiments were carried out using a smooth slope, a slope with a canyon, and a slope with a ridge, giving a total of 9 experiments. The topography was located 2.5 m from the source, but was moved closer (1.5 m) in the roll waves regime experiments, since the flow otherwise would have drained completely before it encountered the topography. The experiments lasted between 4 and 8 hours and ended as the dense source was turned off. Only data from the first 4 hours will be used here since only two experiments lasted more than 4 hours.

The conductivity sensors were calibrated regularly using water with a known salinity. In addition, the bottom and surface density and temperature were measured prior to, and at the end of, each experiment using an Anton Paar DMA35N handheld density meter.

3. Results.

3.1 Flow characteristics and the effect of topography.

As the dense fluid was released, it adjusted and deflected to the left (looking upslope) under the effect of rotation. The dense current flowed with an along-slope velocity component due to rotation and an across-slope velocity component due to friction. The speed of the current was 2 - 5 cm/s, which is smaller than (2). The current width increased from around 30 cm close to the source to a couple of meters downstream, and the thickness of the plume, H_P, varied from a few cm at the source to a few mm downstream. In the laminar regime (Fig. 2a), the interface between the dense current and the ambient fluid was sharp, indicative of little or no mixing. In the waves regime experiments, banded structures appeared in the dense current and moved on the slope at an angle similar to that of the current. Darker crests and lighter troughs can be seen in Fig. 2b. As the structures moved downslope, they grew in amplitude but did not break in the three-dimensional fashion observed by Cenedese and Adduce (2008). Finally, in the eddy regime experiment (Fig. 2c), cyclonic eddies formed in the water above the dense current and moved along-slope with a small across-slope velocity component. Dense fluid was trapped below the eddies, and the domes so formed are seen in dark color in Fig. 2c.

When a canyon or a ridge was present on the slope, it channeled the dense current downslope (see Fig. 2c). The plume became narrower and thicker, and accelerated as it flowed downslope alongside the canyon/ridge. The source flow Q_0 was smaller than the transport capacity Q_C of the ridge/canyon (Wåhlin, 2002; Darelius and Wåhlin, 2007), and the entire plume was steered downslope by the topography. In all regimes, irregularities or instabilities could be seen developing along the walls of the canyon/ridge (Fig. 2d) and moving alongside the topographic feature.

3.2. Salinity in the basin.

Figure 3 shows the salinity in the basin as a function of time and depth for the laminar experiment. Also inserted are black dashed lines showing the reference thickness, $h(t)$, that the plume water would have if there was no mixing at all. This thickness is obtained as

$$\int_{0}^{h(t)} A(z)dz = Q_0 t ,$$ (3)

where $A(z)$ is the basin area as a function of distance above bottom and Q_0 is the source volume flux. In the present experiments $A(z) = A_0 + \Gamma z$ where $A_0 = 15 \ m^2$ and $\Gamma = 76 \ m$, and $Q_0 = 10 \ l/\min$. Inserting these expressions into (3) gives

$$h(t) = -\frac{A_0}{\Gamma} + \sqrt{\frac{A_0^2}{\Gamma^2} + 2\frac{Q_0 t}{\Gamma}} .$$ (4)

There is a certain time-lag corresponding to the time it takes for the dense water to reach the conductivity probes (see Fig. 1c), and the dashed lines representing $h(t)$ have been shifted so that t = 0 when the water first reaches the probes.

When there is no small-scale topography present, almost undiluted source water is deposited at the bottom of the basin in a thickening layer. The dense interface oscillates, presumably because of internal waves that travel across the basin on the dense interface. When a ridge or a canyon is present on the topography, a larger volume of less dense water is found in the basin. This shows that more ambient fluid has been entrained compared with the experiment without small-scale topography.

4. Mixing induced by the topographic features.

The dense water drained downslope either by the frictional Ekman transport, or it was channeled into the basin by the topography. Although the actual drainage scale appeared to be somewhat larger than (1), it was smaller than the length of the slope (8 m) and the plume did not collide with the wall at the left end (looking upslope) of the slope. It is believed that the observed dilution of the source water was caused by plume entrainment processes on the slope itself. Because of the intrinsic time variability, the time-lag discussed in the previous section, and the slight difference in the measurements between the two probes, some precaution is required to estimate the entrainment. The last measurement was taken immediately after the source water was stopped, hence the volume of plume water in the basin can not be used to calculate the total entrainment since measurements were not taken after the whole dense water volume reached the basin. However, the mixing can be estimated from the dilution of the plume density compared to its source value. It is tempting to take the average of the measurements at the two probes and to low-pass filter the data in order to reduce the variability. Such a procedure 'creates' artificial mixing since the profiles then become smoothed compared to the original data. Instead a bulk mixing ratio r_B has been obtained in a similar manner as in Cenedese et al. (2004). First, a mean plume density anomaly $\Delta\rho_P$ was calculated from the last profile at $t = t_f$, $\rho(t_f, z) = \rho_F(z)$ using

$$\Delta\rho_P h_B = \int_0^D (\rho_F(z) - \rho_A)dz \,.$$

In the above, ρ_A is the ambient background density and h_B the thickness of the plume water layer in the basin calculated from the last profile, defined as the level where the density first exceeded ρ_A by $0.001 \ kg/m^3$ or more. Next, r_B was calculated by dividing $\Delta\rho_P$ with the source density anomaly $\Delta\rho_0 = \rho_0 - \rho_A$,

$$r_B = \frac{\Delta\rho_P}{\Delta\rho_0}\,.$$

Finally, the average of the mixing ratio from the two probes was calculated. The results are shown in Table 2. No mixing gives $r_B = 1$, and complete mixing gives $r_B = 0$. As can be seen, the mixing ratio is smallest (i.e. more mixing) for the waves regime and largest (i.e. less mixing) for the laminar regime, in agreement with Cenedese et al. (2004). When topography is present on the slope, r_B decreases in all regimes. The largest topography-induced decrease in the mixing ratio is found in the experiments with the canyon topography.

A bulk estimate of the total entrained transport, Q_E, is obtained from the expression (Cenedese et al, 2004)

$$Q_E = Q_0(\frac{1}{r_B} - 1)\,.$$

A mean value of the entrainment velocity w_E is then given by

$$w_E = \frac{Q_E}{A_P}\,, \tag{5}$$

where A_P is the total surface area of the plume (see Table 2). Assuming that the plume

velocity U is approximately equal to the Nof speed (2), the entrainment coefficient E, defined by $w_E = EU$, can be calculated using (5) and (2),

$$E = \frac{Q_E}{U_N A_P}. \tag{6}$$

The results are shown in Table 2. In order to compare the obtained E with previous studies a representative value of the Froude numer Fr_B,

$$Fr_B = \frac{U_N}{\sqrt{g' H_P}},$$

where H_P is the plume thickness, was estimated. The plume thickness varies between 2 cm at the source down to the Ekman layer thickness (1.3 mm) in the drainage layer, and these values gave the upper and lower values of Fr_B quoted in Table 2. Upper and lower estimates of the bulk Reynolds number, Re_B, were obtained in a similar manner, i.e.

$$Re_B = \frac{U_N H_P}{\nu}.$$

The obtained values for E, Fr_B, and Re_B conform quantitatively to those reported in Cenedese and Adduce (2008). However, it should be stressed that these values are obtained using plume thicknesses that vary considerably as the plume descends the slope, giving a range of Fr and Re that vary over an order of magnitude (Table 2). Furthermore, the Nof velocity (2) may be a good approximation for the flow near the source, but the flow descending the slope in the viscous Ekman layer is probably slowed significantly by bottom friction. Hence, it is debatable how representative the bulk values of E, Fr_B, and Re_B are.

All three regimes show evidence of increased mixing in the presence of a submarine topography, probably induced by the instabilities that were observed downslope the ridge/canyon (e.g. Fig. 2d). Theoretical estimates of plume velocity and thickness in the vicinity of the ridge/canyon (Darelius and Wåhlin, 2007; Wåhlin 2002) can be used to estimate a topographic Froude number Fr_T. This has been done in the Appendix by using the source density and spatial averages of the velocity and thickness from the analytical model. The results are shown in Tables 2 and 4. The topographic Froude and Reynolds numbers are larger than the slope values, which may explain the enhanced entrainment rates that were observed.

The plume water was divided into four density classes defined by r_B (see Table 3). The volume of each density class in the basin has been calculated from the salinity profiles. The result is shown in Figs. 4 - 6, where the percentage of the volume, up to 30 cm depth, that each density class occupies is plotted as a function of time. There are no abrupt changes in the rate of increase of each density class, indicating that the mixing processes were constant during the experiments and that no regime shift occurred.

As expected, the volume of 'pure' basin water decreases with time as it is replaced by plume water. In the laminar regime (Fig. 4), the experiments with a canyon and a ridge have a larger and more rapidly increasing volume of 'highly diluted' and 'moderately diluted' source water than the experiment with smooth topography. There is less 'pure' source water produced in the experiments with a canyon/ridge than without. In the waves regime (Fig. 5), the mixing on the straight slope is enhanced compared with the laminar regime. This can be seen by comparing Figs. 4d and 5d; there is no 'pure' source water produced in the waves regime for the smooth topography but there is in the laminar

regime. Figs. 5b and 5c show that the presence of a ridge or a canyon increased the mixing; there is more 'highly diluted' source water formed with the canyon/ridge topography and more 'moderately diluted' water formed with the smooth topography. In the eddies regime (Fig. 6), the influence of the topography is not as clear. Figure 6d shows that only small volumes of 'pure' source water reaches the basin when the canyon/ridge is present and Fig. 6c that there is somewhat more 'moderately diluted' source water compared with the smooth topography. There is no clear difference between the topographies in the production of 'highly diluted' source water.

In all regimes the canyon induces more mixing than the ridge and, as can be seen in Table 2, the canyon also has larger theoretical Froude and Reynolds numbers than the ridge. The nine experiments show mostly similar results for the two probes, but there are certain differences. For example it can be seen in Figs. 4c and 6c that the densest water is recorded at C5. This may be caused by the Ekman drainage before the canyon/ridge that transports nearly unmixed water down to the probe.

5. Discussion.

The present study quantitatively confirms previous experiments concerning plume entrainment and dynamics for flow on a smooth slope (e.g. Lane-Serff and Baines, 1998; Cenedese et al, 2004). Furthermore, it was observed that both the entrainment rate and the total entrainment increased when a ridge or a canyon was placed on the slope. Enhanced mixing caused by tidal flow over submarine canyons has previously been observed for example on the Mid-Atlantic Ridge (e.g. Ledwell et al., 2000), and in the

laboratory (Wells and Helfrich, 2006). However, the mixing process suggested by the present results is not driven by tides, but by the plume water's release of potential energy as it flows downslope. In the vicinity of the ridge or canyon, a theoretical plume thickness and velocity can be predicted (Davies et al., 2006; Darelius and Wåhlin, 2007), and have previously been shown to agree with laboratory experiments (Davies et al., 2006; Darelius, 2008). In the present experiments, the theoretically predicted Froude and Reynolds numbers for the topographically steered flows were larger than for the flow on the smooth slope.

In the present study, the smooth slope flow has a small Reynolds number (less than 1000) compared with those for the ocean flows. However, our measurements show that also in the experiments with the lowest bulk Reynolds numbers there some mixing is taking place. This is believed to be due to the mechanism observed by Cenedese et al. (2004) and Cenedese and Adduce (2008). In those studies, roll waves were observed to induce mixing in a dense plume descending a slope in a rotating system. Roll waves are a manifestation of a bottom drag[1] induced instability, and appear in shallow flows. As they descend the slope, they grow in amplitude and they can break in a three dimensional fashion, which greatly increases the mixing (Cenedese and Adduce, 2008). However in the present study the roll waves traveled across the slope at a constant speed without breaking, much like those observed by Cenedese et al. (2004).

When the dense flow enters the canyon/ridge region, it thickens and other mechanisms can induce mixing. An initially laminar low-Reynolds number flow accelerating down the canyon/ridge region may develop Kelvin-Helmholtz instabilities, leading to

---

[1] As shown in Cenedese et al. (2004), the bottom drag coefficient can be defined by $C_D = 1/Re$, hence relating frictional drag with molecular viscosity. This definition of the drag coefficient is found to be a good approximation at low Reynolds numbers (Tritton 1988).

overturning and turbulence. As observed by Baines (2001) and Davies et al. (2002), this creates small-scale mixing of the flow at the interface between the ambient fluid and the descending gravity current. The onset of these shear-driven instabilities is governed primarily by the Richardson number. Previous work by Davies et al. (2002) on intrusive gravity currents into stratified ambient fluids demonstrated that background rotation has negligible effect on this mixing and that the dominant parameter controlling entrainment and mixing is the Froude number. The increased mixing in the canyon/ridge flows can also be explained by breaking roll waves, which lead to a turbulent flow and induce an enhanced mixing (as observed in Cenedese and Adduce, 2008). Cross-sectional photographs could not be obtained inside the canyon/ridge area, and we can not discern which of these mechanisms was active in increasing the mixing in the topographically steered flow. Both breaking roll waves and Kelvin-Helmholtz instabilities will increase mixing as *Fr* and *Re* are increased. What can be discerned however, is that the flow enters a new regime when it is topographically steered, and as a consequence the plume entrainment changes. It seems likely that this may also happen in the ocean. The present results suggest that when a canyon or a ridge induces topographic steering, the small-scale topography will affect the mixing properties of the outflow and also the basin density and stratification. There are presently no models available that capture these small-scale processes and that can be used, for example,.in subgrid parameterizations of dense overflows. More field data is clearly needed in order to assess whether topographic steering of dense water is indeed an agent that is of importance to the ocean stratification.

Appendix

The dynamics governing topographically steered plume flows were described in Wåhlin (2002; 2004), Davies et al. (2006) and Darelius and Wåhlin (2007), where an analytical 1.5 layer model, assuming a first-order force balance between the pressure gradient, the Coriolis, and the frictional forces, was employed. Flow in a v-shaped canyon was first considered in Davies et al. (2006). Figure 7 shows a sketch of the canyon flow, with the thickness of the layer given by

$$h(y) = \begin{cases} H_0 \left[\dfrac{1}{\gamma} - \dfrac{1}{\gamma} e^{-\gamma} e^{\gamma y/W} \right] & -W \le y < 0 \\[2mm] H_0 \left[\left(\dfrac{2}{\gamma} - \dfrac{1}{\gamma} e^{-\gamma} \right) e^{\gamma y/W} - \dfrac{1}{\gamma} \right] & 0 \le y < Y_R \\[2mm] 0 & y < -W, y \ge Y_R \end{cases} \qquad (7)$$

In the above $d(y)$ is the bottom elevation, $h(y)$ is the thickness of the dense layer, $\gamma = \dfrac{sW}{\delta}$, s is the slope of the canyon axis, W is the 'effective' width of the canyon defined as the distance between the locations where the dense layer intersects the left canyon wall (looking upslope) and the middle of the canyon (see Fig. 7), $\delta = \sqrt{\dfrac{2\nu}{f}}$ the Ekman depth, $Y_R = -\dfrac{W}{\gamma} \ln\left(\dfrac{1}{2 - e^{-\gamma}} \right)$ is the position where the dense layer intersects the right canyon wall (looking upslope) and H_0 is the height at which the dense layer intersects the left canyon wall (looking upslope). These geometrical definitions are shown in Fig. 7.

Similarly, the layer thickness for flow leaning on a v-shaped ridge is given by

$$h(y)+d(y) = \begin{cases} 0 & y < -W \\ H_0 \left[\dfrac{1}{\gamma} - \dfrac{1}{\gamma} e^{-\gamma} e^{-\gamma y/W} \right] & -W \le y \le 0 \\ H_0 \left(\dfrac{1}{\gamma} - \dfrac{1}{\gamma} e^{-\gamma} \right) e^{-\gamma y/W} & y > 0 \end{cases} \tag{8}$$

The maximum downward flow, Q_C, that can be supported by the ridge or canyon is obtained when the canyon/ridge is completely 'filled', i.e. H_0 is the height of the ridge/canyon and W its width. The geostrophic transport is given by

$$Q_G = \int_{-\infty}^{\infty} h(y) v_G(y) dy, \tag{9}$$

where v_G is the geostrophic velocity along the ridge/canyon. Using (7) and (8) in (9) gives Q_C for the canyon,

$$Q_C^{Canyon} = \frac{g'}{f} H_C^2 \frac{1}{\gamma_C^2} (2e^{-\gamma_C} - 2 + \ln(2e^{\gamma_C} - 1)),$$

where H_C is the canyon depth, $\gamma_C = \dfrac{sW_C}{\delta}$ and W_C is the canyon width. For the ridge we have

$$Q_C^{Ridge} = \frac{g'}{f} H_R^2 \frac{1}{\gamma_R^2} (\gamma_R - 1 + e^{-\gamma_R}),$$

where H_R is the ridge height, $\gamma_R = \dfrac{sW_R}{\delta}$ and W_R is the ridge width. Using the kinematic viscosity of water $v = 10^{-6} \, m^2/s$ and $f = 0.21 \, s^{-1}$, we obtain $\delta = 1.3 \, mm$. Using the experiments geometrical values $H_{C/R} = 10$ cm, $W_{C/R} = 8$ cm, and s = 0.1, we obtain

$\gamma_{C/R} = 5.2$ and $Q_C^{Canyon} = 0.0014 \dfrac{g'}{f}$ m^3/s and $Q_C^{Ridge} = 0.0016 \dfrac{g'}{f}$ m^3/s, which give the values quoted in Table 1 when evaluated with the appropriate g'.

The obtained canyon/ridge transport capacities are larger than the source volume flow for all experiments, and as expected all the water in the plume was steered down by the canyon/ridge. To obtain the theoretical plume thickness and velocity in the ridge/canyon flow, H_0 was found through iteration using the source flux, $Q_0 = 10$ l/min, and the transport capacity Q_C. The results are listed in Table 4. Figure 7 shows the estimated position of the interface and the velocity for the waves regime.

For each experiment the theoretical Froude number, Fr_T, was calculated using the lateral mean values of the theoretical layer thickness, $\overline{h}$, and the velocity, $\overline{u}$. In order to obtain a representative mean value, this was calculated in the area where $h > 0.5 \cdot h_{max}$, where h_{max} is the maximum thickness of the dense layer (the area is shaded in Figure 7). The results are presented in Table 2 and Table 4.

The Reynolds number, Re, can be written as

$$\text{Re} = \frac{uh}{v}. \tag{10}$$

For each experiment the theoretical Reynolds number, Re_T, was also calculated using the lateral mean values of the theoretical layer thickness, $\overline{h}$, and the velocity, $\overline{u}$. The results are presented in Table 2 and Table 4.

References:

Baines, P. 2005. Mixing regimes for the flow of dense fluid down slopes into stratified environments. Journal of Fluid Mechanics, 538, 245-267.

Baines, P. 2001. Mixing in flows down gentle slopes into stratified environments. Journal of Fluid Mechanics, 443, 237-270.

Baines, P. G. and S. Condie (1998). Observations and Modelling of Antarctic Downslope Flows: a Review. Ocean, Ice, and Atmosphere - Interaction at the Antarctic Continental Margin. S. S. Jacobs and R. F. Weiss. Washington D.C., AGU. 75.

Baines, P. and J. Turner, 1969. Turbulent buoyant convection from a source in a confined region. Journal of Fluid Mechanics, 37, 51–80.

Cenedese, C., Whitehead, J.A., Ascarelli, T.A., Ohiwa, M., 2004. A dense current flowing down a sloping bottom in a rotating fluid. Journal of Physical Oceanography, 34, 188−203.

Cenedese, C. and Adduce, C. 2008. Mixing in a density driven current down a slope in a rotating fluid. Journal of Fluid Mechanics, submitted.

Chang, Y. S., Xu, X., Özgökmen, T. M., Chassignet, E. P., Peters, H., Fischer, P. F., 2005. Comparison of gravity current mixing parameterizations and calibration using a high-resolution 3D nonhydrostatic spectral element model. Ocean Modelling, 10, 342 - 368.

Darelius, E. and Wåhlin, A. K., 2007. Downward flow of dense water leaning on a submarine ridge. Deep Sea Research I, 56 (7), 1173 - 1188.

Darelius, E., 2008: Topographic steering of dense overflows - laboratory experiments with vee-shaped ridges and canyons. Deep Sea Research I, submitted.

Darelius, E., Smedsrud, L., Østerhus, S., Gammelsrød, T., Foldvik, A., 2008. On the structure and variability of the Filchner overflow plume. Tellus, submitted.

Davies, P A, Guo, Y & Rotenberg, E (2002) Laboratory model studies of Mediterranean outflow adjustment in the Gulf of cadiz. Deep Sea Research II, 49 (19), 4207-4225

Davies, P., Wåhlin, A. and Guo, Y, 2006. Laboratory and Analytical Model Studies of the Faroe Bank Channel Deep-Water Outflow. Journal of Physical Oceanography, 36, 1348 - 1364.

Ellison, T.H. and Turner, J.S., 1959. Turbulent entrainment in stratified flows. Journal of Fluid Mechanics, 6, 423–448.

Foldvik, A., Gammelsröd, T., Österhus, S., Fahrbach, E., Rohardt, G., Schroder, M., Nicholls, K., Padman, L., Woodgate, R., 2004. Ice shelf water overflow and bottom water formation in the Southern Weddell Sea. Journal of Geophysical Research, 109 (C2).

Girton, J.B., Sanford, T., 2003. Descent and modification of the overflow plume in the Denmark Strait. Journal of Physical Oceanography, 33, 1351–1364.

Hughes, G. and R. Griffiths, 2006. A simple convective model of the global overturning circulation, including effects of entrainment into sinking regions. Ocean Modeling, 12, 46 - 79.

Jiang, L. and R. W. Garwood (1998). Effects of topographic steering and ambient stratification on overflows on continental slopes: A model study. Journal of Geophysical Research 103 (C3), 5459-5476.

Kämpf, J. 2005. Cascading-driven upwelling in submarine canyons at high latitudes. Journal of Geophysical Research, 110, C02007.

Kämpf, J. and H. Fohrmann, 2000: Sediment-Driven Downslope Flow in Submarine Canyons and Channels: Three-Dimensional Numerical Experiments. Journal of Physical Oceanography, 30, 2302 - 2319.

Lane-Serff, G. and P. Baines, 1998. Eddy formation by dense flows on slopes in a rotating fluid. Journal of Fluid Mechanics, 363, 229 - 252.

Ledwell JR, Montgomery ET, Polzin KL, St Laurent LC, Schmitt RW, Toole JM, 2000. Evidence for enhanced mixing over rough topography in the abyssal ocean. Nature, 403, 179-182.

Price, J. F. and O'Neil Baringer, M. 1994. Outflows and deep water production by marginal seas. Progress in Oceanography, 33, 161 - 200.

Sherwin, T. J., Griffiths, C. R., Inall, M. E., and Turrell, W. R. (2008). Quantifying the overflow across the Wyville Thompson Ridge into the Rockall Trough. Deep-Sea Research I (in press).

Sherwin, T. J., and Turrell, W. R. (2005). Mixing and advection of a cold water cascade over the Wyville Thomson Ridge. Deep-Sea Research I, 52(8), 1392-1413.

Smith, P. C. (1975). Streamtube Model For Bottom Boundary Currents In Ocean. Deep-Sea Research, 22 (12), 853-873.

Sutherland, B.R., Nault, J., Yewchuk, K. & Swaters, G.E. 2004 Rotating dense current on a slope. Part1. Stability. J. Fluid Mech., 508, 241-264.

Tritton, D. J., 1988: Physical Fluid Dynamics. Clarendon Press, 519 pp.

Wells J.R., Helfrich K.R., 2006. Mixing at the head of a canyon: A laboratory investigation of fluid exchanges in a rotating, stratified basin. Journal of Geophysical Research, 111 (C12). Art. No. C12004.

Wells, M. and J. Wettlaufer, 2005. Two-dimensional density currents in a confined basin. Geophysical and Astrophysical Fluid Dynamics, 99 (3), 199–218.

Wells, M. and J. Wettlaufer, 2007. The long-term circulation driven by density currents in a two-layer stratified basin. Journal of Fluid Mechanics, 572, 37 - 58.

Vilibic, I., Grbec, B., and Supic, N. (2004). Dense water generation in the north Adriatic in 1999 and its recirculation along the Jabuka Pit. Deep-Sea Research I, 51 (11), 1457-1474.

Wåhlin, A. K., and Cenedese, C. (2006). How entraining density currents influence the stratification in a one-dimensional ocean basin. Deep Sea Research II, 53, 172-193.

Wåhlin, A. K., 2002. Topographic steering of dense water with application to submarine canyons. Deep-Sea Research I, 49, 305–320.

Wåhlin, A. K. 2004. Downward channeling of dense water in topographic corrugations. Deep-Sea Research I, 51, 577–590.
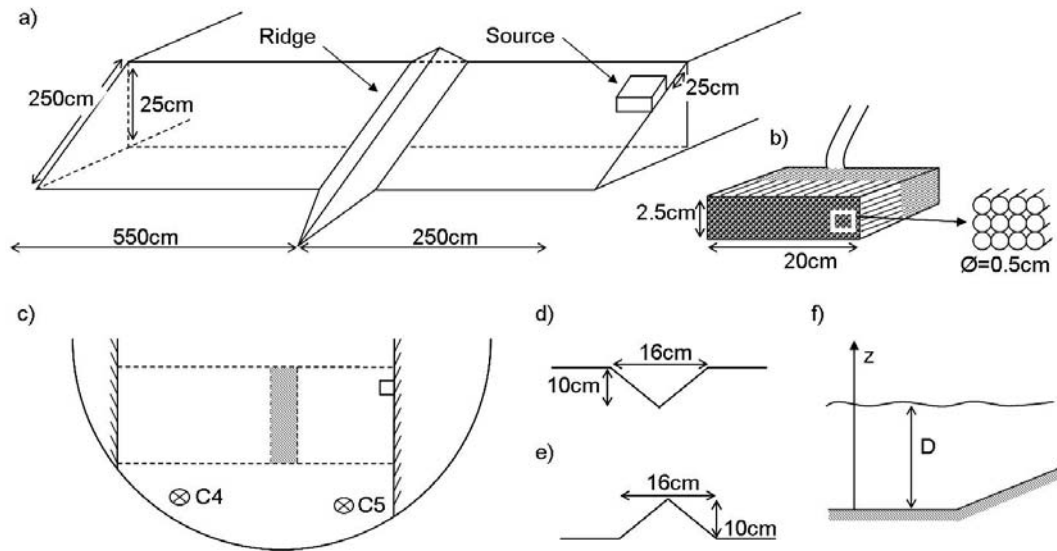
Figures.

Figure 1. Sketch of the experiment set-up (not to scale). a) Overview of the topography, b) Dense source, c) Top view. C4 and C5 mark the position of the vertically traversing probes. Side view of d) the canyon e) the ridge, and f) the shelf

Figure 2. Top view photographs from the 3 regimes. The black marks on the middle of the slope are 1 m apart. The color variation from weaker, on the left side, to stronger on the right side, may be due to a non-uniform illumination. a) Laminar regime, b) Waves regime, c) Eddies regime (the plume is here steered downslope by a canyon) d) Instabilities forming alongside the ridge wall.
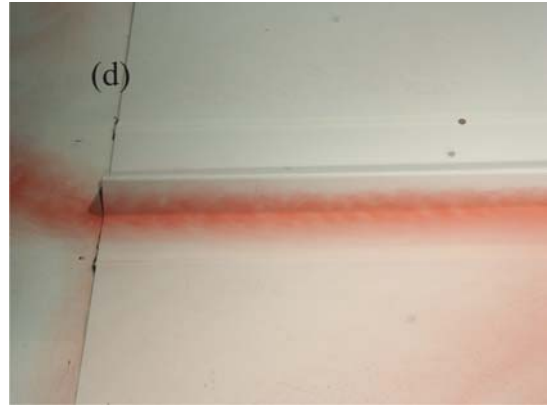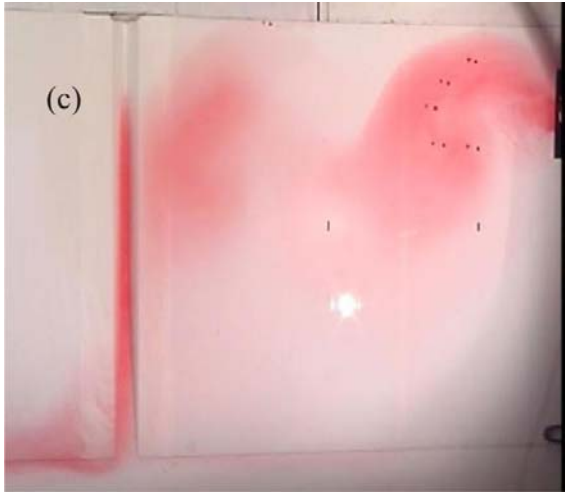
Figure 3. Salinity as a function of time (min) and distance above bottom (m) for the laminar experiment with (a) smooth topography, (b) ridge and (c) canyon. Colors indicate salinity according to the colorbar, the scale has been adjusted so that red is pure source water (i.e. S = 10.8 in (a), S = 7.7 in (b) and S = 7.1 in (c)) and blue is pure basin water (i.e. S = 5.8 in (a), S = 1.8 in (b) and S = 1.8 in (c)). Black dashed line shows the reference level at which the interface would be if there was no mixing between plume and ambient water. The curve has been shifted so that t = 0 at the time when the dense fluid first reaches the conductivity probes. Only data from probe C4 is shown. White areas indicate missing data.
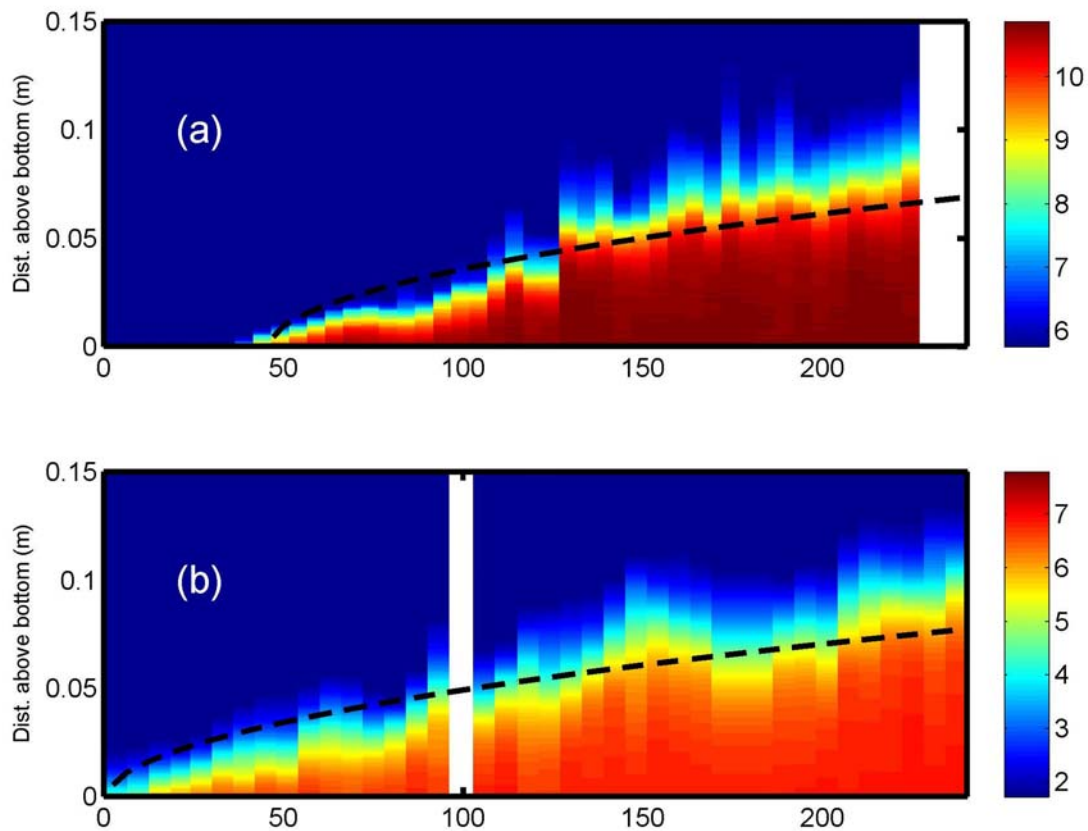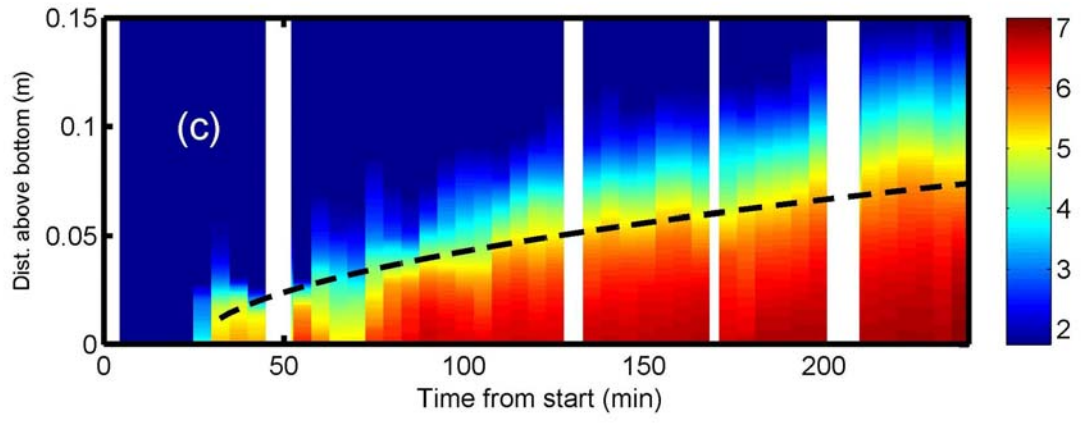
Figure 4. Volume of water within the four density classes as a function of time. Data from the laminar experiments with smooth topography (green), ridge topography (red) and canyon topography (blue). Circles show data from C4, triangles data from C5. (a) Basin water (b) Highly diluted source water (c) Moderately diluted source water (d) Pure source water.
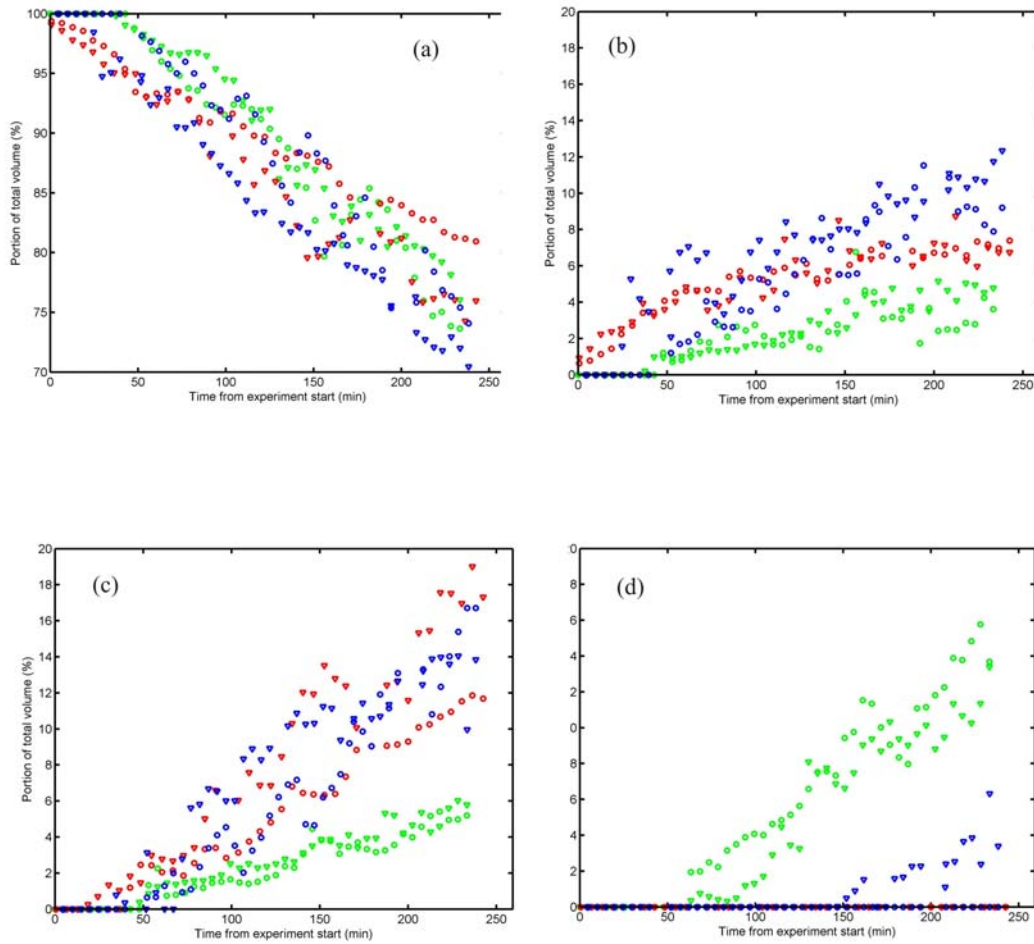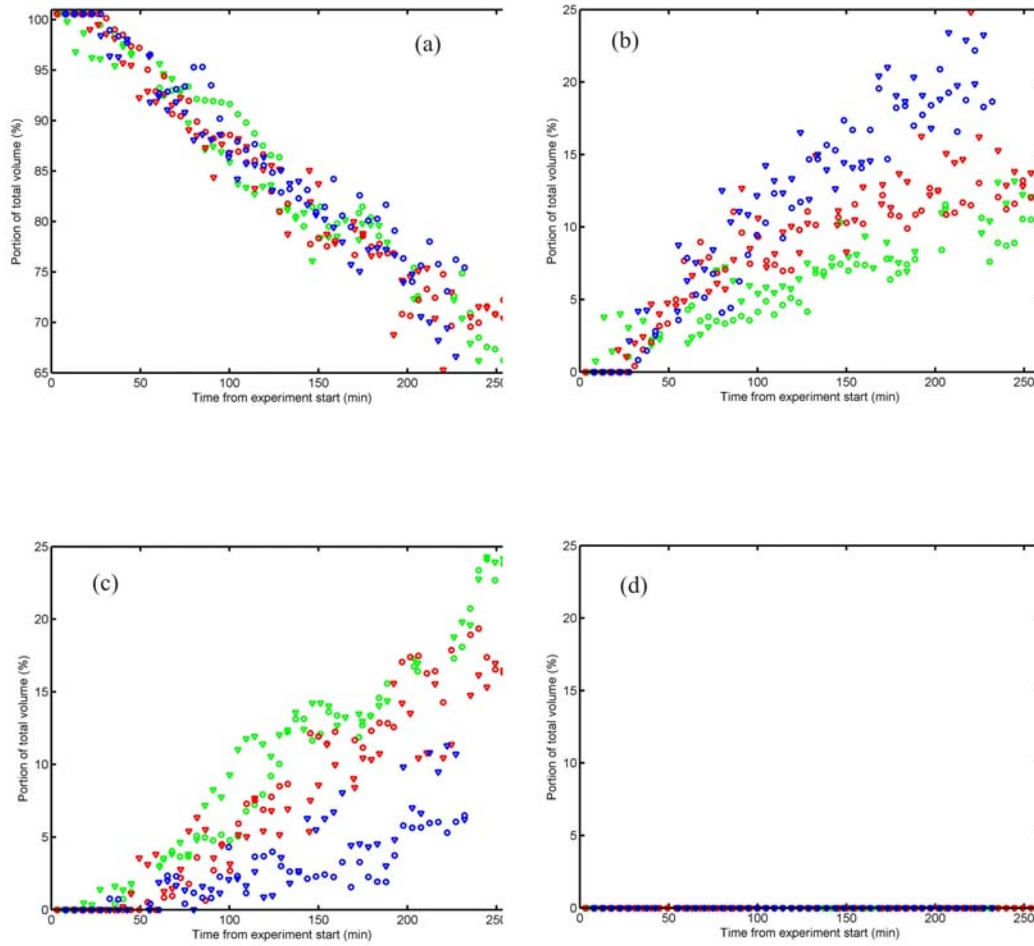
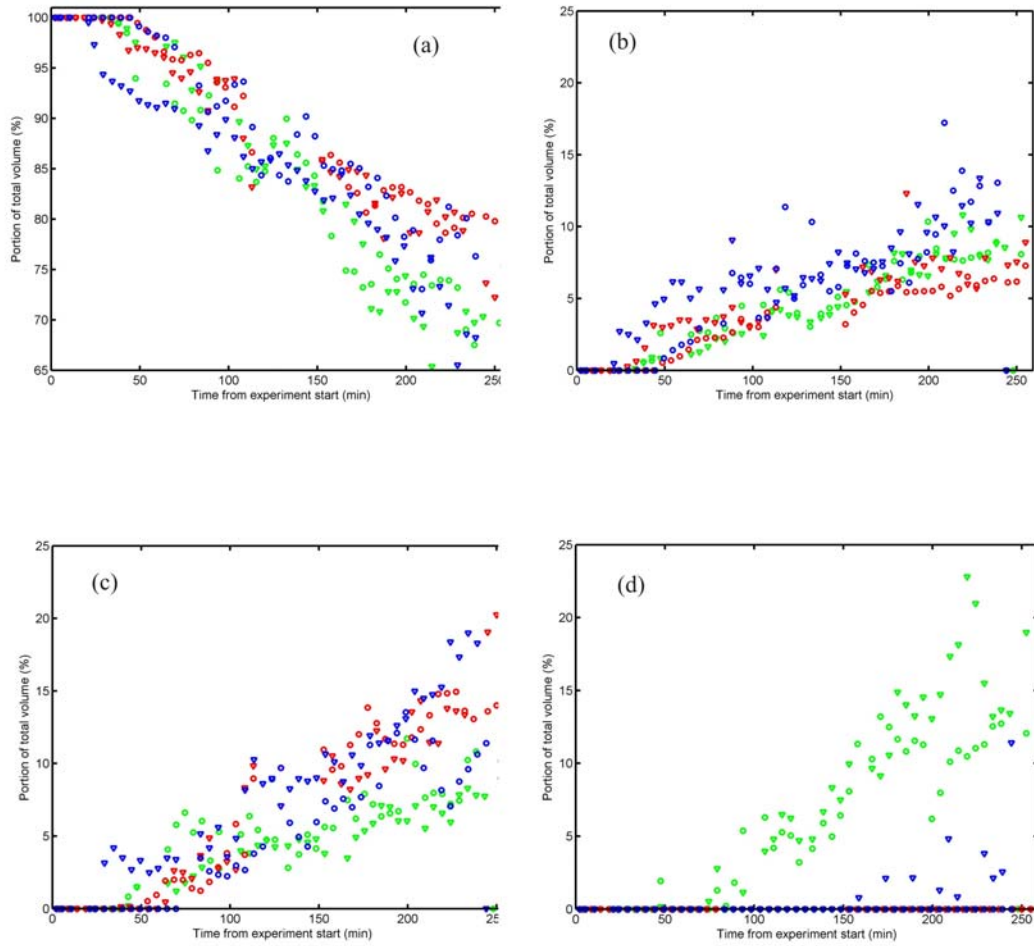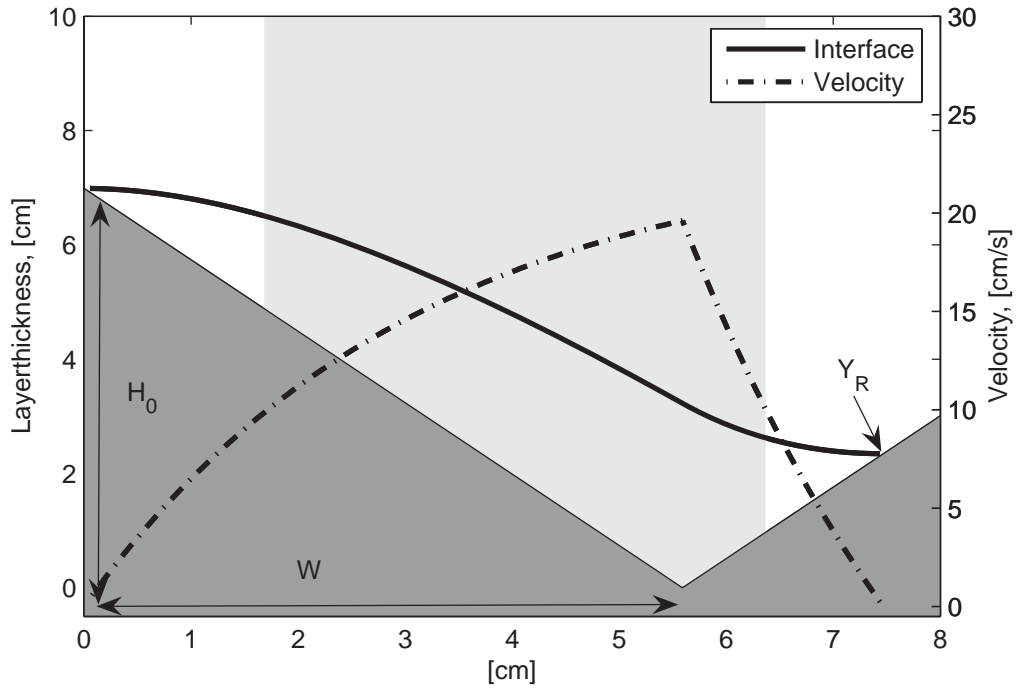**Figure 5**. Same as in Fig. 4, but for the waves regime.

Figure 6. Same as Fig. 4, but for the eddies regime.

Figure 7. Estimated interface position and geostrophic velocity for the waves regime. The grey shading indicates the area from which values are used in the calculation of mean thickness and velocity.

Tables.

Table 1: Values of ambient water depth (D), source density difference ($\Delta\rho_0$) and derived parameters drainage length (L_D), transport capacity (Q_C) and Nof velocity (U_N).

Regime	Topography	D (cm)	$\Delta\rho_0$ (kg/m^3)	L_D (m)	Q_C (l/min)	U_N (cm/s)
Laminar	Straight	65	3.7	2.9	0	1.7
Laminar	Ridge	65	4.4	2.4	19	2.1
Laminar	Canyon	65	3.9	2.8	16	1.8
Waves	Straight	35	11	1.1	0	5.1
Waves	Ridge	35	9.4	1.1	41	4.4
Waves	Canyon	35	9.2	1.2	37	4.3
Eddies	Straight	35	4.3	2.9	0	2.0
Eddies	Ridge	35	4.3	2.9	19	2.0
Eddies	Canyon	35	3.1	3.5	13	1.5

Table 2. Mixing ratio (r_B), surface area (A_P), entrainment coefficient (E), bulk Froude number (Fr_B), topographic Froude number (Fr_T), bulk Reynolds number (Re_B) and topographic Reynolds number (Re_T) for the different regimes and topographies.

Regime	Topography	r_B	Q_E (l/min)	A_P (m^2)	E $\cdot 10^{-4}$	Fr$_B$	Fr$_T$	Re$_B$	Re$_T$
Laminar	Smooth	0.76	2.4	9	2.6	0.6-2.5		30-300	
Laminar	Ridge	0.63	3.7	5	5.9		4.7		3400
Laminar	Canyon	0.60	4.0	5	7.4		4.9		3700
Waves	Smooth	0.54	4.6	5	3.0	1.1 - 4.3		100-1000	
Waves	Ridge	0.50	5.1	3	6.4		6.4		4400
Waves	Canyon	0.44	5.6	3	7.2		6.9		6200
Eddies	Smooth	0.70	3.0	15	1.5	0.7 - 2.7		40 - 400	
Eddies	Ridge	0.59	4.1	5	6.8		4.7		3400
Eddies	Canyon	0.56	4.4	5	9.6		4.9		3700

Table 3. Definition of the water masses studied in Figs. 4 - 6.

Density class	Mixing ratio r_B	Basin water (% of total volume))
Basin water	< 0.3	> 70
Highly diluted source water	0.3 - 0.7	30 - 70
Moderately diluted source water	0.7 - 0.95	5 - 30
Pure source water	> 0.95	<5

Table 4. Interface height (H_0) defined in the appendix, mean height $\bar{h}$ and velocity $\bar{u}$ derived from the theoretical model together with reduced gravitational acceleration g' and the topographic Froude number Fr_T and Reynolds number Re_T for the experiments with topography.

Topography	H_0 (cm)	$\bar{h}$ (cm)	$\bar{u}$ (cm/s)	g' (m/s^2)	Fr_T	Re_T
Canyon	7.0	2.5	15	0.04	4.9	3700
Canyon	4.4	2.0	31	0.1	6.9	6200
Ridge	5.9	2.4	14	0.04	4.7	3400
Ridge	3.4	1.7	26	0.1	6.4	4400